Optical properties of high aspect ratio plasma etched silicon nanowires: fabrication-induced variability dramatically reduces reflectance

2015 Nanotechnology 26 085301

(http://iopscience.iop.org/0957-4484/26/8/085301)

IOP Publishing Nanotechnology
Nanotechnology 26 (2015) 085301 (12pp) doi:10.1088/0957-4484/26/8/085301

Optical properties of high aspect ratio plasma etched silicon nanowires: fabrication-induced variability dramatically reduces reflectance

A Smyrnakis[1,2], E Almpanis[1,3], V Constantoudis[1], N Papanikolaou[1] and E Gogolides[1]

[1] Institute of Nanoscience and Nanotechnology, NCSR 'Demokritos', Aghia Paraskevi, 15310, Greece
[2] School of Chemical Engineering, National Technical University of Athens, Zografou, 15780, Greece
[3] School of Applied Mathematical and Physical Science, National Technical University of Athens, Zografou, 15780, Greece

E-mail: e.gogolides@inn.demokritos.gr

Received 13 November 2014, revised 18 December 2014
Accepted for publication 9 January 2015
Published 3 February 2015

Abstract

In this work we investigate both experimentally and theoretically the optical properties of aligned, perpendicular to the substrate, high aspect ratio (AR), plasma etched Si nanowires (SiNWs) with controlled variability. We focus on the role of imperfections in fabrication, which manifest themselves as dimensional variability of SiNW, lattice defects or positional randomization. SiNW arrays are fabricated by e-beam lithography (perfectly ordered array) or colloidal particle self-assembly (quasi-ordered array) followed by cryogenic Si plasma etching, which offers fast etch rate (up to 3 μm min^{-1}) combined with clean, smooth, and controllable sidewall profile, but induces some dimensional variability on the diameters of the SiNWs. Sub-200 nm diameter SiNWs having AR as high as 37:1 are demonstrated. The total reflectance of SiNWs is below 2% in a wide range of the optical spectrum. We experimentally demonstrate improved light absorption when moving from a perfectly ordered (after e-beam lithography) to a defective and quasi-ordered (after colloidal self-assembly) SiNW array. In addition our measured reflectivity (for both ordered and quasi-ordered SiNWs) is much lower compared to the one predicted theoretically for a perfect SiNWs array, using full-electrodynamic calculations with the layer-multiple-scattering method. To explain such low reflectivity, we model the influence of disorder using the average *T*-matrix approximation and show that even small dimensional variability (10–20%) leads to dramatic reduction of the reflectance (matching the experimental results) and increased light trapping inside the SiNW justifying their possible application in photovoltaic devices.

Keywords: silicon nanowires, plasma etching, cryogenic etching, antireflective surfaces, optical simulation, multiple scattering, lithography

(Some figures may appear in colour only in the online journal)

1. Introduction

Silicon micro- and nanowire (SiNW) arrays with controlled sizes and period are promising for high performance nano-devices such as energy conversion devices, photodiodes, chemical and biological sensors, lithium batteries and field effect transistors, due to their unique structural, electrical and optical properties [1, 2]. In particular, SiNWs can offer several advantages for photovoltaic applications as silicon is an abundant, stable and non-toxic material with an almost ideal

energy bandgap and compatible with modern microelectronics industry. The use of SiNWs in solar cell devices has been recently reviewed by several groups [3–7]. The two basic approaches for the fabrication of SiNWs include the bottom-up and the top-down approach [8]. Bottom up methods include the vapor–liquid–solid growth (VLS method) [9], which makes use of metal (Au,Cu) as catalyst and gaseous Si precursor (SiH_4) [10, 11]. Several works on solar cells based on SiNW growth have been demonstrated [12–15]. The main drawback of the VLS method is the metallic contamination [16] that can lead to minority-carrier lifetime and diffusion length degradation. The top-down approach is based on pattern definition followed by etching for pattern transfer. For the pattern definition, top-down lithographic methods (such as optical, interference, e-beam, nanoimprint lithography etc) or bottom-up self assembly methods, such as colloidal particle self-assembly (colloidal or nanosphere lithography) [17] can be used. Then, pattern transfer to silicon is performed by either wet etching, such as the newly developed metal-catalyzed electroless etching [3, 18, 19], or dry plasma etching processes.

Plasma etching is a standard Si nanofabrication process that can be used to fabricate highly uniform, well-defined perpendicular to the substrate SiNWs. In particular, plasma etching may be valuable for making SiNWs on cheaper Si films deposited on glass or other substrate in order to reduce the cost [20]. Several plasma chemistries can be used to etch silicon. The cryogenic process (employing a gas mixture of SF_6 and O_2 at temperatures usually below −100 °C) and the room temperature time-multiplexed alternating processes, such as the Bosch process, are commonly used when deep reactive ion etching is required [21]. Especially, for SiNW and nanopillar fabrication both approaches with some variations have been demonstrated [22–25]. When deep etching is not needed, mixed fluorocarbon processes, chlorine or bromine based processes can also be used [26]. Details about the cryogenic silicon plasma etching process can be found in [27–31].

As mentioned before, there is an increasing interest for the use of SiNWs in photovoltaic applications. The surface reflection is one of the most significant factors for optical loss in Si solar cells. Perpendicular to the substrate periodic SiNW arrays exhibit low reflection and strong optical absorption [32–34], which can be useful in a photovoltaic device. The optical properties of periodic SiNWs have been calculated theoretically, and their absorption enhancement has been recognized [35, 36]. SiNW arrays have lower reflectance than Si thin films of the same thickness [35]. For example, tapered SiNW, or nanotips with diameter variation along their height enhance antireflectivity [37, 38]. Moreover, simulation studies have been performed by Lin *et al* [39] and Li *et al* [40] to give guidelines for the optimum nanowire design characteristics for the best optical absorbance. Theoretically, it has been reported that structural disorder and randomness can result to optical absorption enhancement, which is attributed to the stronger optical scattering in a random structure [39, 41–43]. More specifically, position randomness [39] but more importantly wire diameter and length deviations [41] have been predicted to significantly increase broadband absorbance in freestanding SiNW.

In previous works we studied the mechanical and antiwetting properties of plasma etched SiNWs (room temperature nanoBosch process) [25] and their application as templates for bioinspired three-dimensional ZnO/Si nanoarchitectures [44]. Here we present a systematic experimental and theoretical study of SiNW optical properties, focusing on the role of their positional randomization and especially their dimensional variability. We report a top-down approach for the fabrication of aligned and perpendicular to the substrate high aspect ratio (AR) SiNWs by cryogenic Si plasma etching (section 3.1). The optical properties of SiNWs of different diameter, height, periodicity and order are evaluated by measuring the total, specular and diffuse reflectance. We compare (for the first time to our knowledge) the optical response of ordered and quasi-ordered SiNW arrays fabricated by e-beam lithography and the cost-effective colloidal lithography respectively (section 3.2). In addition, we perform full-electrodynamic calculations using the layer-multiple-scattering (LMS) method to analyze the optical response of the SiNWs, and we employ the average *T*-matrix approximation (ATA) to study the dimensional variability effects on the SiNW optical properties. We will demonstrate that the experimental results of reflectance can be matched to our theoretical calculations only when variability in the nanowire diameter is taken into account. We theoretically predict that dimensional variability as low as 10–20% (realistically present in various etching processes) is enough to reduce reflectance to levels well below 20% even for a perfectly periodic array (section 3.3). We conclude that small imperfections in lithography and mainly plasma etching result in dimensional variability, which is enough to reduce reflectance and increase light absorbance of SiNWs.

2. Experimental details

2.1. SiNW fabrication

The substrates used were n-type (100) Si wafers with resistivity ranging from 1 to 5 Ω cm. Colloidal particle self-assembly was performed by spin coating a monolayer of closely-packed polystyrene (PS) spheres on the silicon substrate. The process of colloidal lithography is described in detail by Ellinas *et al* [24]. Two different particle sizes were used: 1000 nm diameter PS spheres (purchased from Microparticles GmbH, catalog number PS-R-L1343, 10%w/v aqueous suspensions, ⩽3% CV) and 520 nm diameter PS spheres (purchased from Distrilab, catalog number 5052A, 10%w/w aqueous suspensions, ⩽3% CV). After the coating, an isotropic O_2 plasma etching step was performed to shrink the PS spheres to the desirable diameter. The plasma conditions were: helicon high density plasma tool (MET system, Adixen working in inductive mode) with source power 1900 W, pressure 1.33 Pa, 100 sccm O_2 flow at temperature 15 °C, no bias power. In addition, e-beam lithography (Vistec EBPG5000plusES) was employed to pattern dot arrays

arranged in a square or hexagonal lattice using a hydrogen silsesquioxane (HSQ) negative tone resist.

After pattern definition, SiNWs were fabricated by cryogenic silicon plasma etching using a SF_6/O_2 gas mixture at cryogenic temperature. Depending on the pattern used, the samples were etched in the same plasma reactor (as above) at −105 °C, source power of 1000–1200 W and bias generator power 35 W (this corresponds to −55 V bias voltage). The gas flows were 200 sccm SF_6 and 40–60 sccm O_2 at a pressure of 1.33 Pa. Temperature was controlled by helium backside cooling of a carrier Si wafer covered with a thick (>50 μm) SU-8 film on which samples were glued with thermal paste. PS spheres were removed after etching in a toluene bath followed by acetone ultrasonic bath and propanol bath. The SiNW morphology characterization was performed by scanning electron microscopy measurements on a JSM 7401F instrument from Jeol. SEM image analysis have been performed using the homemade software CERDEMO [45], which uses top-down images for the evaluation and characterization of contact edge roughness .

2.2. Reflectance characterization

The reflectance (total, specular and diffuse) of the SiNWs was measured using a ThetaMetrisis FR-Reflection kit which includes an Ocean Optics ISP-50-GT Integrating Sphere coupled to an Ocean Optics QE65000-ABS UV–NIR Spectrometer. A combination of a deuterium and a tungsten lamp was used as light source covering the spectra range from 200 to 1000 nm. The light excitation in the integrating sphere is angled at 8°. The integrating sphere is also equipped with a trap that fits into a hole angled at −8° and is coated with either a black absorbing material or with the same material as the sphere that allows one to disintegrate the specular and the diffuse part of the total reflectance. A high-reflectivity specular reflectance standard (STAN-SSH-NIST) from Ocean Optics calibrated to a NIST master was used as a reference.

2.3. Computational method

The theoretical study of the optical response of assemblies of SiNWs is performed through full-electrodynamic calculations using the LMS method, which has been presented in detail elsewhere [46–48]. In brief, the method can deal with structures consisting of successive, possibly different, layers of scatterers arranged with the same 2D periodicity. At a first step, in-plane multiple scattering is evaluated in a spherical-wave basis using proper propagator functions. Subsequently, interlayer scattering is calculated in a plane-wave basis through appropriate reflection and transmission matrices. The scattering S matrix of a multilayer slab, which transforms the incident into the outgoing wave field, is obtained by combining the reflection and transmission matrices of the individual component layers, allowing the description of composite structures, which are used in an actual experiment, and include e.g. an array of scatterers standing on a supporting substrate forming a fully absorbing surface [49]. In order to ensure convergence in our calculations for the structures of SiNWs on a Si substrate we truncate the spherical-wave expansion at $\ell_{\max} = 16$ and take into account 109 2D reciprocal lattice vectors in the relevant plane wave expansion. The single-particle scattering T-matrix is evaluated with $\ell_{\text{cut}} = 20$.

The multiple scattering method is essentially a technique to solve the Maxwell differential equations and works very efficiently in cases where we consider periodic arrays of structures embedded in a homogeneous medium, similar to the SiNWs we consider in this work. The method is based in the division of space in closed regions (scatterers) and the solution is found in two steps. First we solve the problem of a single scatterer which for the problem at hand is obviously a SiNW in free space. For a collection of cylinders, waves scattered out from one cylinder will be scattered again from another etc. All these multiple scattering events can be summed up, in a second step, elegantly and efficiently in case of periodic structures. This separation of the multiple scattering problem allows for a systematic treatment of substitutional disorder in arrays of periodic scatterers within the ATA, which has been originally introduced for the study of the electron properties of disordered metals and surfaces [50, 51], appropriately adapted for the calculation of optical properties of random 2D and 3D arrays of scatterers [52, 53].

A full solution of the electric field scattered by a single Si cylinder can be directly obtained through the scattering T-matrix which is analytical in case of spherical scatterers, and can be numerically obtained in case of cylinders [46] in a spherical wave expansion. Assuming an electric field $\mathbf{E}(\mathbf{r}, t) = \Re\mathrm{e}[\mathbf{E}(\mathbf{r})\exp(-\mathrm{i}\omega t)]$ can be written in a spherical wave expansion around a scattering center:

$$\mathbf{E}(\mathbf{r}) = \sum\nolimits_L \left[\frac{\mathrm{i}}{k} a_{E;L} \nabla \times j_\ell(kr)\mathbf{X}_L(\hat{\mathbf{r}}) + a_{H;L} \nabla \times j_\ell(kr)\mathbf{X}_L(\hat{\mathbf{r}}) \right], \quad (1)$$

where $k = n\omega/c$ is the wavenumber, $\mathbf{X}_L(\hat{\mathbf{r}})$ are the vector spherical harmonics with $L \equiv (\ell, m)$ being the angular momentum combined index, and $j_\ell(kr)$ is the spherical Bessel function, while $a_{E,H;L}$ are appropriate expansion coefficients. A similar expansion can be written for the outgoing scattered wave by replacing the spherical Bessel function with outgoing Hankel functions. The spherical expansion coefficients of the scattered waves denoted $a^{+}_{E,H;L}$ can be connected to the coefficients of an incoming incident wave $a^{0}_{E,H;L}$ through the scattering T-matrix for the individual scatterer i:

$$a_i^{+} = \mathbf{T}^i(\omega) a_i^{0}. \quad (2)$$

In a lattice of cylinders the scattering of each cylinder depends on the exact geometrical arrangement of the cylinders around it. This is correctly accounted for within multiple scattering theory, since all phase information between scattering events is taken into account. For a periodic array of cylinders with a random distribution of sizes we could neglect scattering between different cylinders, and try to find an approximate description, assuming a periodic structure with

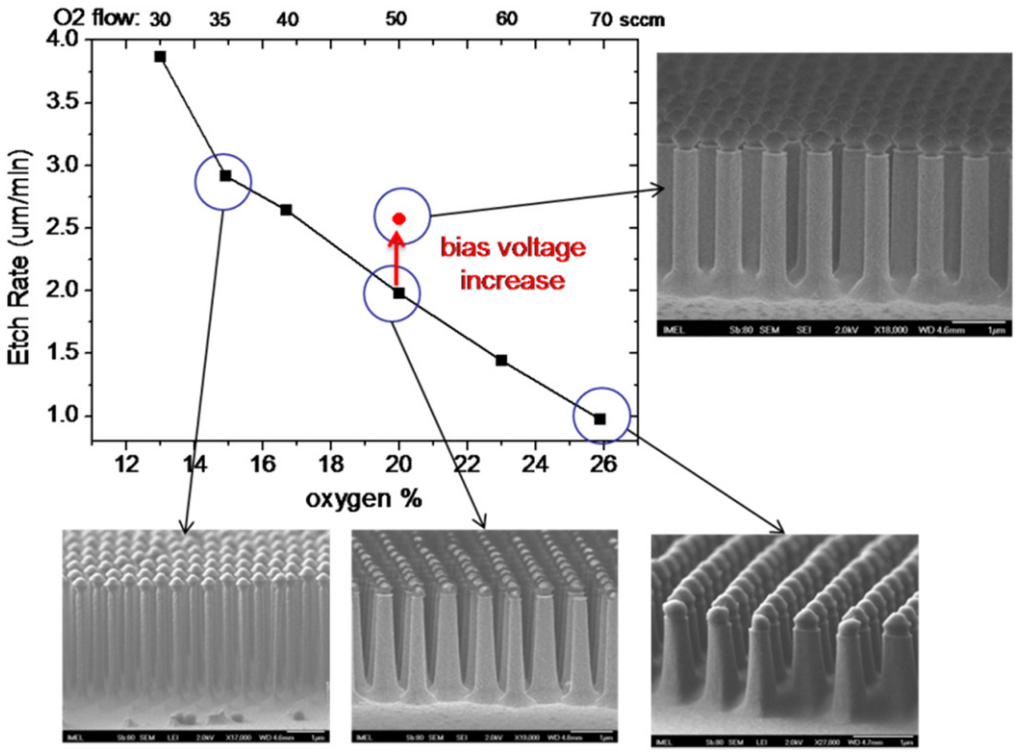

Figure 1. Silicon etch rate in cryogenic etching process versus O_2 percentage in the SF_6/O_2 gas mixture or O_2 gas flow. The corresponding SEM images of Si pillars patterned by colloidal lithography keeping the same period and diameter are presented. The plasma parameters are: temperature = −105 °C, source power: 1200 W, bias voltage: 30–55 V, pressure: 10 mTorr, SF_6 flow: 200 sccm and O_2 flow: 30–70 sccm.

'average scatterers,' ignoring the phase information between scattering events (random phase approximation). Therefore, for a random distribution of N types of cylinders with different geometrical characteristics the average T-matrix is given by:

$$\langle \mathbf{T} \rangle = \sum\nolimits_N C_N T^N, \tag{3}$$

where C_N is the fraction of the different cylinder types, while $\sum C_N = 1$. The method is simple to implement within the layer multiple scattering theory and could be systematically improved by more sophisticated but complex coherent potential approximations [51]. The ATA approximation is more appropriate for systems with a relatively small randomness.

3. Results and discussion

3.1. Fabrication of SiNWs

The main tool for the top-down fabrication of the SiNWs is the cryogenic silicon etching process. In previous works, we demonstrated the use of cryogenic process after e-beam lithography [44] and after colloidal lithography for the fabrication of SiNWs with ARs up to 18:1 [24]. Here, we further optimize the cryogenic process in order to achieve even higher ARs, offering fast etch rates and higher selectivity over the mask material. The role of each plasma parameter (such as O_2 gas flow or bias voltage) on the SiO_xF_y sidewall passivation layer and the quality of etching has been nicely presented by de Boer *et al* [28]. Figure 1 shows silicon etch rate versus O_2 gas flow or O_2 percentage in the SF_6/O_2 gas mixture, and the corresponding SEM images (samples patterned by colloidal lithography). Increasing O_2 percentage from 13% to 26% decreases etch rate from 3.8 to 1 μm min^{-1}, eliminates undercut, and results in positively sloped silicon pillars due to overpassivation. At 20% (or 50 sccm O_2 flow), an increase in the bias generator power (bias voltage increase from 30 to 55 V) gives the desired vertical sidewall profile. Due to the increase of the ion energy, the sidewall profile turns from positively sloped to fully vertical with almost zero undercut. Note that at the bottom of the pillars a pyramid-shaped base is present. This is due to crystal orientation dependent etching (CODE) [31]. As reported in other works [54, 55], (111) planes appear at the bottom because the etch rate of Si(100) is larger than that of Si(111). The effect of this conical base in the optical properties will be analyzed and discussed in more detail in the following section.

The passivation layer formed during the cryogenic etching is volatile at room temperature and as a result the sidewalls of the fabricated SiNWs and pillars are clean, and smooth with very low surface roughness, while the profile can be fully controlled. We managed to have fast etch rates (2.5–3 μm min^{-1} depending on the mask pattern used) and high etch selectivity over different etching mask materials. In particular, the measured selectivity for our cryogenic process are 85:1 for the AZ photoresist, 45:1 for the PMMA, 140:1

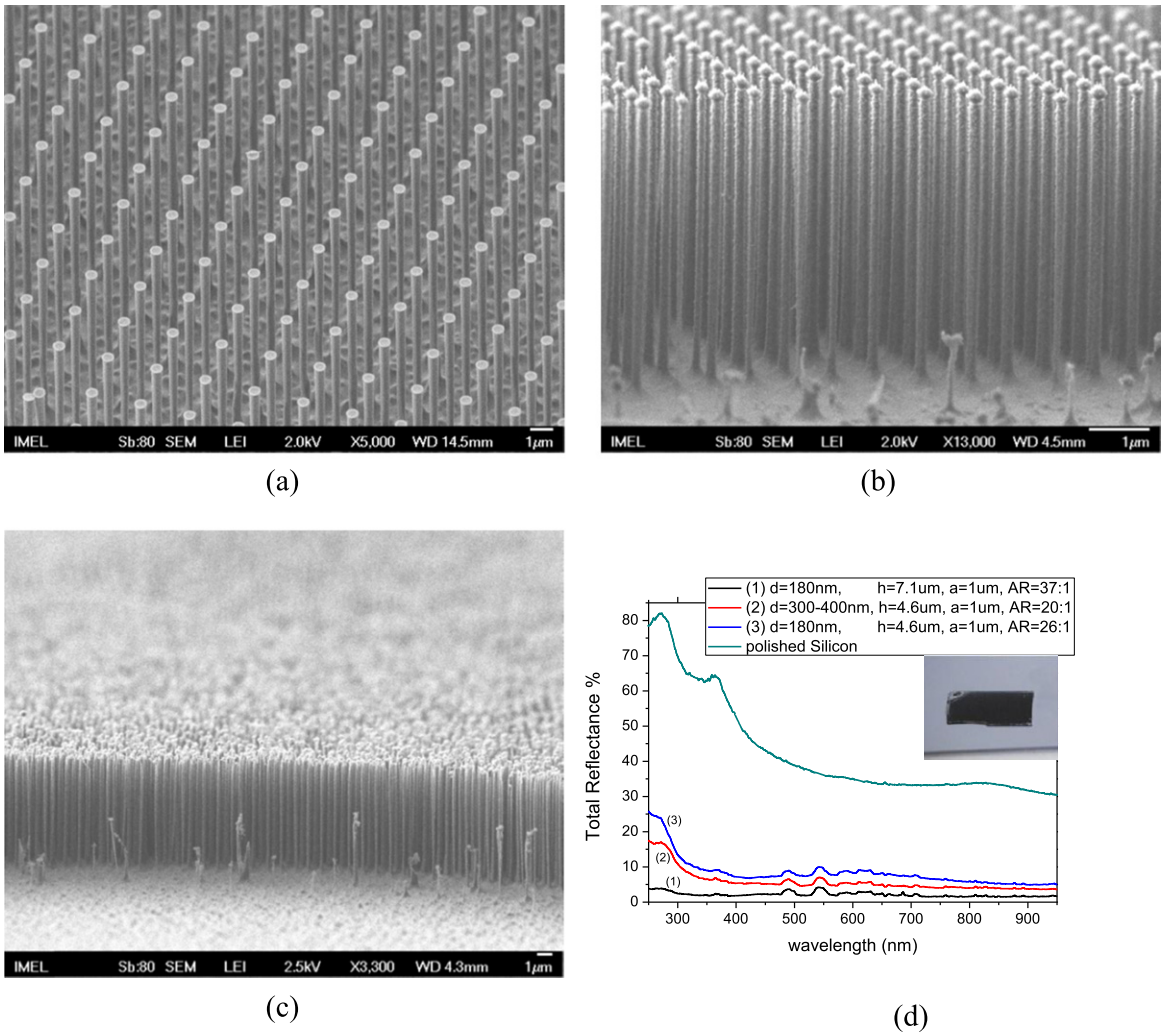

Figure 2. SEM images of plasma-etched silicon nanowires (SiNWs) patterned by (a) e-beam lithography (aspect ratio (AR) of 20:1, $d = 440$ nm, $h = 8.9$ μm, period $a = 2$ μm, tilted 45°), (b) colloidal particle self-assembly (AR = 26:1, $d = 180$ nm, $h = 4.62$ μm, $a = 1$ μm, tilted 70°), and (c) colloidal particle self-assembly (AR = 37:1 $d = 180$ nm, $h = 7.13$, $a = 1$ μm, tilted 70°). (d) Total reflectance of a Si surface with perpendicular high aspect ratio SiNWs of various dimensions (colloidal particle self-assembly has been used to define SiNW position) compared to the reflectance of a polished Si wafer. Inset: Photograph of a nanostructured sample on a polished Si wafer.

for the PS and over 300:1 for the SiO_2. As a consequence there is no need of using hard metal mask to fabricate high AR nanostructures. In figure 2, periodic perpendicular to the substrate high AR SiNWs fabricated by the cryogenic process are demonstrated. Figure 2(a) shows SiNWs with a diameter of 440 nm and AR 20:1, patterned by e-beam lithography and arranged in a rectangular lattice with period 2 μm. Figures 2(b) and (c) show SiNWs patterned by PS colloidal particle self-assembly with diameter ~180 nm and AR of 26:1 and 37:1, respectively. They are arranged in a hexagonal lattice with a period of 1 μm, as a result of the colloidal sphere pattern.

3.2. Optical characterization of SiNW

Reducing reflectance is an essential element in photon management for possible application such as energy harvesting devices and photovoltaics. This is usually done by inserting an intermediate 'effective' refractive index (n_{eff}) to avoid the abrupt transition at the Si/air interface, typically a thin antireflection coating. Several antireflection schemes have been reported [56]. Nanostructured surfaces with SiNWs with a periodicity similar to the wavelength of the incident light can also act as homogeneous medium with an intermediate effective refractive index that depends on NW period, diameter, length, and filling fraction [57]. As a result, the use of SiNWs can reduce the reflectance at the Si/air interface, enhance the light trapping and improve the collection and absorption of incident photons. In figure 2(d) the total reflectance of high AR SiNW arrays of different diameter and height (as shown in figures 2(b) and (c)) is presented in comparison with the total reflectance of a polished silicon wafer surface. A significant reduction of the reflectance compared to the polished silicon surface is observed. For the same diameter and period of the hexagonal lattice, nanowires with higher AR show lower reflectance. The total reflectance is reduced below 2% in a wide range of the optical spectra for the higher AR SiNWs. In addition, the specular reflectance is

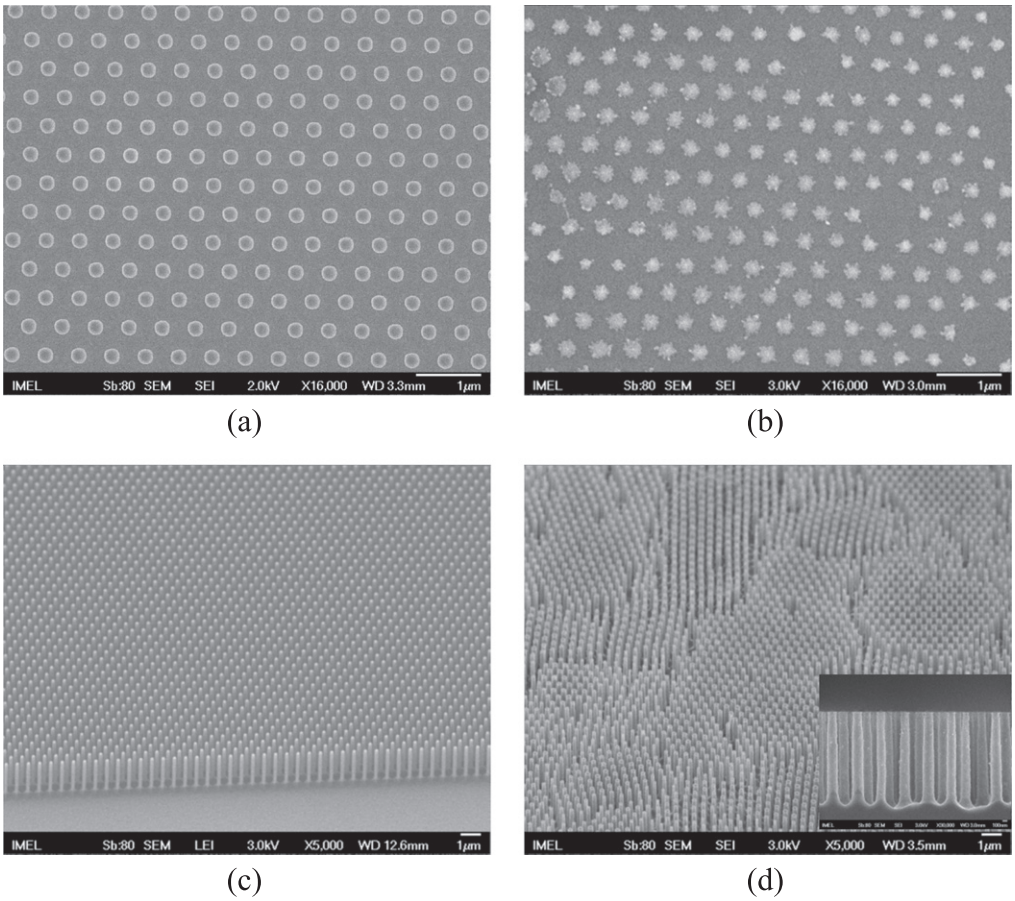

Figure 3. (a)–(b) Top-down SEM image of a hexagonally ordered dot mask pattern on Si as a result of e-beam lithography and colloidal polystyryne particle self-assembly, respectively. The period of the pattern is 520 nm and the mean diameter is ∼240 nm. (c)–(d) Result of the pattern tranfer for the fabrication of SiNW by cryogenic etching using the mask patterns of (a) and (b) respectively. The height of the SiNWs is 2.1 μm and the SEM images are tilted at 45°. Embedded the corresponding cross-section SEM image is presented.

reduced below 1%. As a consequence, these nanostructured samples look black in the naked eye, as seen in the inset of figure 2(d).

The process of colloidal lithography as a self-assembly method imports defects in the hexagonal lattice in which the coated spheres are arranged, which are transferred as order defects of the SiNW arrays. These defects can be dislocations of the lattice or vacancies where a particle may be missing. Moreover, defects such as a deviation in the final colloidal sphere diameter and a roughness around every sphere are produced in the isotropic oxygen plasma step. To make a direct comparison of the role of these lattice defects and disorder in the reflectance, e-beam lithography was employed to pattern a large area of 1 cm^2 of fully ordered SiNW array without any defect. Figures 3(a) and (b) show top-down SEM images of hexagonally ordered dot mask pattern after e-beam lithography (an HSQ resist was used) and colloidal PS particle self-assembly, respectively. The two patterns have the same period of 520 nm and the same mean diameter of approximately 240 nm. To ensure that the two patterns are of the same diameter SEM image analysis was performed to find the diameter and its variation using the CERDEMO software developed and available from our group [45]. Results are shown in table 1, and reveal a large deviation (19.4% with respect to the mean diameter, or $3\sigma = 45.6$ nm) for the colloidal lithography spheres, and a small deviation (2.1%, or $3\sigma = 4.8$ nm) for the e-beam resist dots. The dots of the pattern from the e-beam lithography have a mean diameter of 233.3 nm while the mean diameter the colloidal particles after the isotropic etching was calculated at 235.6 nm.

Using these two patterns as etching mask, cryogenic etching was employed to fabricate arrays of fully ordered SiNWs in the case of e-beam lithography (figure 3(c)) and quasi-ordered SiNWs in the case of colloidal lithography (figure 3(d)). The samples were etched simultaneously to ensure that the SiNWs are of the same height (=2.1 μm) and sidewall profile in both cases. As seen in figure 3(c), in the case of e-beam lithography the periodicity and alignment of the SiNWs in the hexagonal lattice is perfect. On the contrary, in figure 3(d) some dislocations and 'cracks' appear in the lattice, a result of the way the colloidal spheres are spin coated. In the embedded cross-section SEM image we see that there is a thinning at the top side of the SiNWs. Image analysis of top-down SEM images after etching is also shown in table 1. Again, dimensional variability is observed for both samples showing deviation of (18.3%, $3\sigma = 33$ nm) for the colloidal lithography patterned SiNWs (reduced after etching) and 7.1% ($3\sigma = 13.2$ nm) for the e-beam. Notice that the

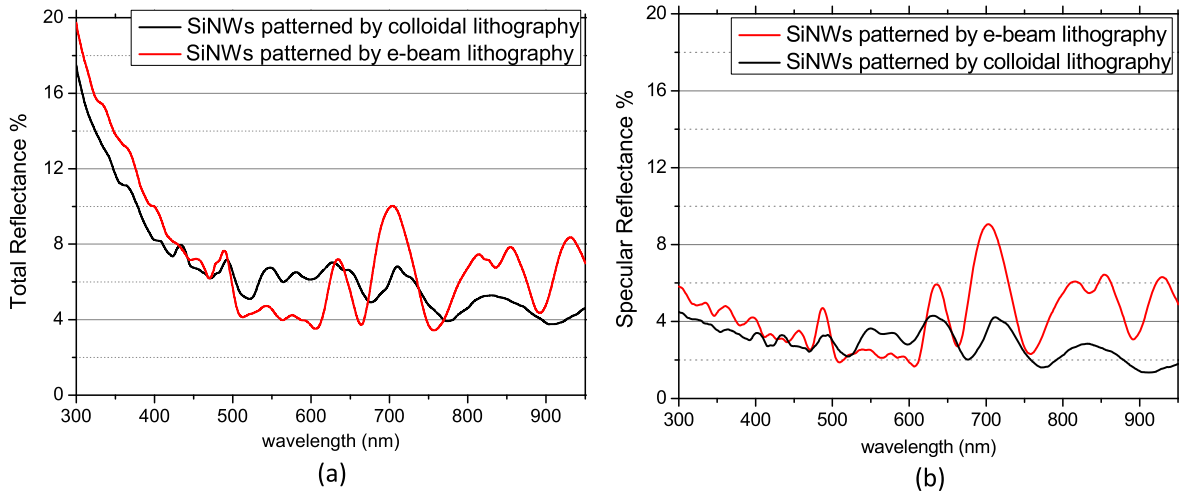

Figure 4. Comparison of (a) the total reflectance and (b) the specular reflectance of fully ordered SiNWs patterned by e-beam lithography and quasi-ordered SiNWs patterned by colloidal particle self-assembly.

Table 1. Mean diameter and standard deviation as calculated by SEM image analysis of the samples shown in figure 3. SEM image analysis was performed using the CERDEMO software developed and available from our group [45].

	Mean diameter $\|d\|$ (nm)	σ (nm)	3σ (nm)	$3\sigma/\|d\|$ (%)	SEM image
colloidal sphere pattern	235.6	15.2	45.6	19.4	3(b)
e-beam dot pattern	233.3	1.6	4.8	2.1	3(a)
SiNW after colloidal	180.0	11.0	33.0	18.3	3(d)[a]
SiNW after e-beam	185.6	4.4	13.2	7.1	3(c)[a]

[a] The corresponding top-down images were used for the analysis.

plasma etching process has significantly increased the variability of the e-beam patterned SiNWs, while it has slightly reduced the variability of the colloidal lithography patterned samples. The mean top diameter of the NWs is 180.0 nm for those patterned by colloidal lithography, and 185.6 nm for those patterned by e-beam lithography. The diameter of the main body of the NWs is approximately 200 nm. Notice also, that at the bottom of every NW the pyramid-like base due to the CODE effect of cryogenic etching appears. The effect that these two morphologies at the top and bottom of the NWs have in the reflectance will be discussed in detail in the following theoretical section.

In figure 4 a comparison of (a) the total reflectance, and (b) the specular reflectance of the ordered and the quasi-ordered SiNW arrays of the same mean diameter, height and period as measured in a integrating sphere is demonstrated. We observe that the SiNWs patterned by the colloidal lithography show lower total and specular reflectance in a wide area of the optical spectra except from the range between 500 and 600 nm. Some reflectance peaks appear at the wavelengths 487, 634, 705, 814 and 854 nm in both cases, but with significantly lower intensity for the quasi-ordered SiNWs. There is little difference between total and specular reflectance (figures 4(a) and (b), respectively) above 520 nm (which is the lattice constant of the array); peaks in this region should be attributed to Mie-type modes of the isolated SiNW (see section 3.3). However, total reflectance is higher than the specular below 520 nm, due to significant contribution of higher diffraction orders. Taking into account that the NW profiles are identical we can experimentally conclude that lattice defects, diameter variability, and positional randomization enhance antireflectivity.

3.3. Theoretical study of optical properties

We have also performed full-electrodynamic calculations using the extended LMS method. We start our analysis from a freestanding periodic array of SiNWs with the geometry suggested by the fabricated structures i.e. diameter $d = 200$ nm and height $h = 2000$ nm arranged in a hexagonal lattice with lattice constant $a = 520$ nm, which is schematically shown in figure 5(a). In all calculations we have considered the Si optical constants [58]. The corresponding calculated reflectance spectrum under normal light incidence is shown with green-solid line in figure 5(e). The spectrum can be roughly divided in two regions. For wavelengths below 650 nm, reflectance of the freestanding SiNWs is rather small and the structure is highly transparent. For longer wavelengths, the simulations predict resonances centered around 700 and 840 nm, which can be attributed to Mie-type modes of the isolated SiNW. According to our calculations, these resonances have little dispersion with the light angle of incidence, and are similar to those generating vivid colors in sparse arrays of SiNWs [59]. Additionally, for wavelengths around 750 nm, sharp dips in the reflectance indicate the existence of guided resonances confined inside the structure [60–63],

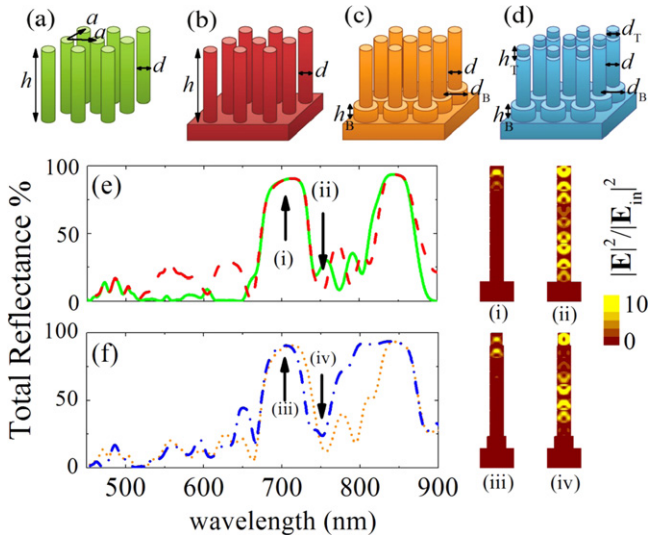

Figure 5. (a)–(d) Schematic of the structures considered in our theoretical analysis. (a) Freestanding array of SiNWs, with $d = 200$ nm arranged in a hexagonal 2D lattice with period $a = 520$ nm. (b) The SiNW array of (a) on top of a semi-infinite Si substrate. (c) Same structure as in (b) but with a modified base, adding a cylinder with $h_B = 200$ nm and $d_B = 280$ nm. (d) Same structure as in (c) but with a modified top adding a cylinder with $h_T = 200$ nm and $d_T = 180$ nm. The total length of the NWs is $h = 2$ μm in all cases. (e) *Green-solid and red-dashed line*: total reflectance for the structure of (a) and (b) respectively. (f) *Orange-dotted and blue-dashed–dotted line*: total reflectance for the structure shown in (c) and (d) respectively. (i)–(iv) Electric field intensity profile for selected resonances, pointed out with arrows in (e) and (f).

which can be attributed to collective guided modes of the array that actually behaves as a photonic crystal slab. Such states leak-out and become quasi-bound due to the periodicity of the structure [64, 65]. Increasing the diameter of the NWs alone leads to a red-shift of the characteristic Mie-type reflectance resonances ~700 and ~840 nm and the guided resonances (not shown here), which is very similar to previous reports [66–68]. Moreover, our calculations confirm that the main features of the spectrum are not very sensitive to small changes of the height of the nanowires. For a given nanowire diameter, small variations in the lattice constant or different periodicity (i.e. square lattice), cause only small spectral shifts and do not modify the optical response of the array significantly.

Adding a semi-infinite Si substrate (figure 5(b)) does not influence the two main Mie-type resonances, as seen in the red-dashed line of figure 5(e). However, we observe a stronger influence of the substrate for wavelengths below 650 nm, since the modes in this spectral region localize the electric field in the area between the nanowires and the substrate [40]. The electric field intensity inside the nanowires of figure 5(b) is shown in figure 5(i)–(ii). The mode around 700 nm has strong electric field intensity mainly in the upper side of the nanowire, which is expected for scattering resonances since the field does not penetrate deep in the structure. On the contrary, the mode around 750 nm shows strong field intensities in the whole nanowire length since it is connected to a guided resonance of the photonic crystal slab that confines light inside the nanowires. Almost all features in the field profiles are present in both structures with and without the substrate.

As discussed previously, the fabricated nanowires have a tapered-like base due to CODE of the cryogenic process and also a thinner top due to etching defects. To account for those features in the theoretical approach, first we introduce a modified nanowire base, by adding a cylinder with larger diameter ($d_B = 280$ nm, height $h_B = 200$ nm), keeping the total height of the SiNW to $h = 2000$ nm, as is schematically depicted in figure 5(c). Interestingly, above 650 nm the corresponding reflectance spectrum in figure 5(f) does not differ much from the one with uniform nanowire structure. A non-ideal base influences mainly the modes induced by the Si-substrate. Next, we add a thinner top in each SiNW using a cylinder with diameter $d_T = 180$ nm and height $h_T = 200$ nm as depicted in figure 5(d). In the reflectance spectrum (blue-dashed–dotted line in figure 5(f)) new resonances appear around 650–700 nm that result in a broadened strongly reflecting band [69]. Considering the field intensities in figure 5(iii)–(iv), we see that the tapered top causes a deeper penetration of the electric field in the Mie-type modes (iii) compared to the untapered SiNW, but without reducing reflectance. The (iv) field intensity which corresponds to a guided resonance of the photonic membrane confines light inside the SiNWs, which is only slightly affected by the tapered base and top. Similar studies of SiNW have been analyzed using an effective refractive index layer between air and Si to account for the suppression of reflectivity [69–73].

There is a significant difference in absolute reflectance values when comparing the theoretically predicted spectra (figure 5) with the experimental results of the fabricated samples (figure 3) which show strong broadband absorption. For example, on the Mie-type resonance at 700 nm, $R_{predicted} = 85\%$ while $R_{measured} = 10\%$. To investigate this, we consider the influence of different kinds of disorder of the fabricated structures on the optical properties. Interestingly, the spectra of the periodically ordered structures obtained with e-beam show already strongly reduced reflectance compared to our theoretical predictions, which is further reduced by the lattice disorder induced by the colloidal lithography. Consequently the origin of the strong absorption of the fabricated SiNW arrays cannot be accounted by the deviation from the periodic arrangement alone. The variation in the diameter of the nanowires, their pyramid-like base, as well as the small tapering of the wire top caused by the etching, should also be considered.

There are few approaches to deal with disorder and variability in the literature. For example an effective index approach was used to account for it in [69], while also averaged spectra of different random arrays to account for random positions, diameters and lengths was also employed. Our theoretical approach goes one step forward in the description of variability by applying the ATA, which treats the averaging in a random phase approximation and neglects intersite correlations between different SiNW. To estimate the effect of variability (dispersion) in the SiNW diameters we assume a random distribution of three types of cylinders with

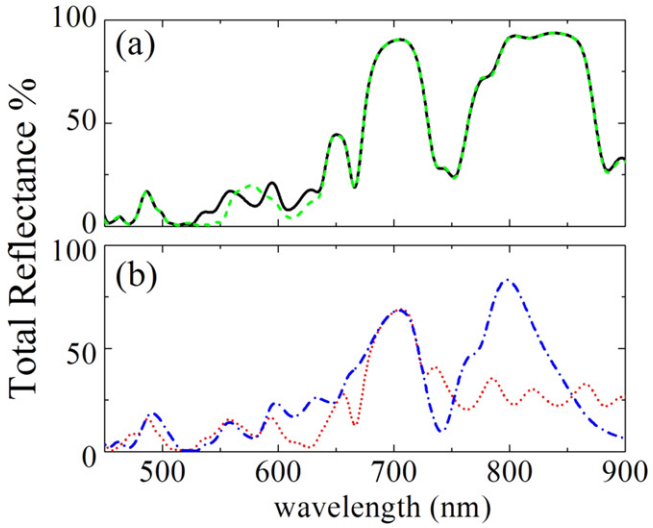

Figure 6. (a) *Black solid line*: total reflectance, under normal incidence of light, for the ordered structure of figure 5(d). *Green-dashed line*: total reflectance for the structure of figure 5(d) using random distribution of three identical cylinders with different base diameters ($0.9d_B$, d_B, $1.1d_B$) keeping all the other geometrical parameters constant. (b) *Blue-dashed–dotted line*: total reflectance for the structure of figure 5(d) using a random collection of three cylinders of different diameters ($0.9d$, d, $1.1d$) for the main body. *Red-dotted line*: total reflectance for the structure of figure 5(d) using a random collection of three identical cylinders of different top diameters ($0.9d_T$, d_T, $1.1d_T$) for the top of the NWs. All the calculations were performed using the ATA.

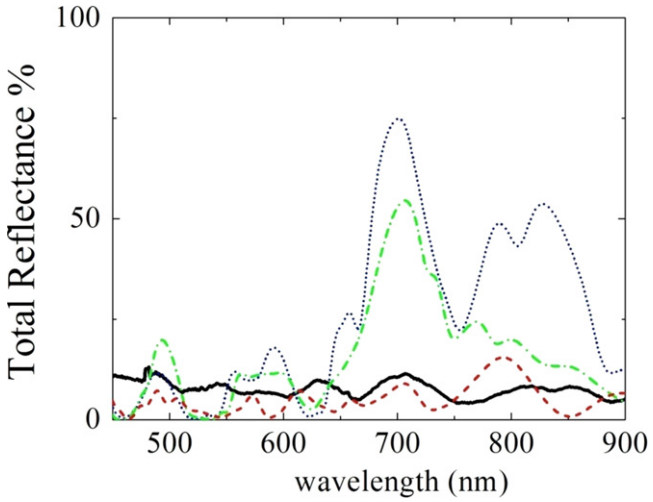

Figure 7. Reflectivity spectrum for the SiNW array of figure 5(d) with diameter variability in all three diameters (top, main body, bottom). Three variation levels of the diameters are shown namely ±5% (blue-dotted line), ±10% (green-dashed–dotted line), and ±20% (red-dashed line), respectively. With black solid line, we plot the measured total reflectance of the fabricated SiNW arrays patterned with e-beam lithography.

equal occupation probability with a 10% deviation from the nominal average diameter $d = 200$ nm of the SiNW. This will allow for a simple quantitative estimate of the effect of variability and disorder on the optical properties. We use a similar procedure by averaging over three types of base and top cylinders assuming a 10% variation in d_B, and d_T. The average T-matrix is given by:

$$\langle \mathbf{T}_D \rangle = \left(\mathbf{T}_{0.9D} + \mathbf{T}_D + \mathbf{T}_{1.1D}\right)/3, \quad (4)$$

where by $\mathbf{T}_D$ we denote the T-matrix of the cylinder with diameter $D = (d, d_B, d_T)$. In figure 6(a) we compare three configurations calculated using the ATA method, with the response of the reference system of figure 5(d). Considering variability in the base only, has little influence on the spectra (green-dashed line in figure 6(a)). The tapered base mainly affects the interface states (between the SiNW array and the substrate) and in order to significantly alter the reflectivity of the whole spectrum one should assume rather stronger variability in the base of the SiNW. The variation of the SiNW diameter d, seems to have a stronger influence and produces the spectrum shown in figure 6(b) with blue-dashed–dotted line. The dominant resonance at 700 nm loses intensity and becomes broader and slightly blue-shifted. A similar intensity reduction is seen for the resonance around 800 nm. Similar ATA results obtained by varying the top diameter by 10% are shown with red-dotted line in figure 6(b). In this case variability introduces a significant reduction in the reflectivity, since tapering the nanowires reduces the optical impedance mismatch between air and Si.

In figure 7 we show the combined effect of of variability using a random collection of cylinders of different diameters for the base, the top and the cylinder diameter. As the dispersion of diameters increases from 5% to 10% and 20% around the nominal diameters, reflectivity is significantly reduced and all the spectral features become broader, giving the correct trend, approaching the experimental observations.

Finally, in order to estimate the amount of the EM energy absorbed by the SiNWs, we calculate the absorption spectrum including variability for the same structure for which reflectivity was calculated (ATA: variability SiNW diameter ±20%). Following [69], we consider a lossless substrate with the same real part as Si and zero imaginary part. The result of both calculations is shown in figure 8, from which we can deduce that the effect of light absorption occurs mainly inside the SiNW, while for the parts of the spectrum where large differences occur (wavelengths between ∼550 and 650 nm), these can be attributed to absorption in the substrate. This estimation is important for the possible application of SiNWs in photovoltaics.

4. Conclusions

A top-down approach for the fabrication of aligned, perpendicular to the substrate, high AR SiNWs with controlled order and variability was presented. Both e-beam lithography (for perfect order) and the cost effective process of colloidal particle self-assembly (for quasi-order) were used followed by cryogenic Si plasma etching. Our fabrication process offers full versatility in wire diameter, height and period showing high anisotropy and high etch rate ($\sim 3\,\mu m\,min^{-1}$), as well as clean, smooth and controllable sidewall profile. Sub-200 nm diameter SiNWs were fabricated with high AR up to 37:1.

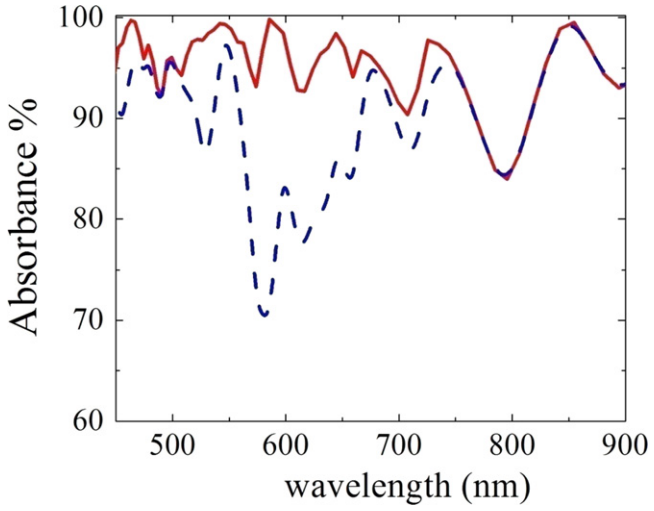

Figure 8. *Red-solid line*: absorbance spectrum for the SiNW array of figure 5(d) with diameter variability. These variations correspond to a disorder in the SiNW diameter ±20%. *Blue-dashed line*: absorbance of the same structure but assuming a lossless substrate.

These nanowires show extremely low total reflectance below 2% in a wide range of the optical spectrum. By comparing reflectance of e-beam and colloidal lithography obtained SiNWs, we experimentally demonstrated that lattice defects, dimensional variability, and positional randomization strongly decrease the reflectance of SiNWs. The LMS method was employed to study the optical response of SiNWs and diameter variability described within the ATA. It is shown that even small (10–20%) dimensional variability mainly of the NW diameters has a key role in the dramatic decrease of the reflectance and increase of the light trapping, matching the experimentally measured reflectance values even for the perfectly ordered SiNW array. We concluded that high AR plasma etching processes, significantly reduce reflectance due to induced dimensional variability as evidenced by SEM metrology analysis. Finally, we predict theoretically that light absorption occurs mainly inside the SiNWs, which is important for their use in photovoltaic devices, a part of our ongoing work. In addition the clean and smooth cryogenic plasma etching may contribute to better electrical properties in terms of lower surface recombination, surface passivation and overall performance.

Acknowledgments

This work was supported by the Research Excellence Project 695 'Plasma Directed Assembly and Organization-Plasma Nano Factory' which is implemented under the 'ARISTEIA I' Action of the 'OPERATIONAL PROGRAMME EDUCATION AND LIFELONG LEARNING' and is co-funded by the European Social Fund (ESF) and National Resources.

References

[1] Wan Y, Sha J, Chen B, Fang Y, Wang Z and Wang Y 2009 Nanodevices based on silicon nanowires *Recent Pat. Nanotechnology* **3** 9
[2] Shao M, Ma D D D and Lee S-T 2010 Silicon nanowires—synthesis, properties, and applications *Eur. J. Inorg. Chem.* **2010** 4264–78
[3] Peng K Q and Lee S T 2011 Silicon nanowires for photovoltaic solar energy conversion *Adv. Mater.* **23** 198–215
[4] Song T, Lee S-T and Sun B 2012 Silicon nanowires for photovoltaic applications: the progress and challenge *Nano Energy* **1** 654–73
[5] Peng K-Q, Wang X, Li L, Hu Y and Lee S-T 2013 Silicon nanowires for advanced energy conversion and storage *Nano Today* **8** 75–97
[6] Kapadia R, Fan Z, Takei K and Javey A 2012 Nanopillar photovoltaics: materials, processes, and devices *Nano Energy* **1** 132–44
[7] Bashouti M Y, Sardashti K, Schmitt S W, Pietsch M, Ristein J, Haick H and Christiansen S H 2013 Oxide-free hybrid silicon nanowires: from fundamentals to applied nanotechnology *Prog. Surf. Sci.* **88** 39–60
[8] Bandaru P R and Pichanusakorn P 2010 An outline of the synthesis and properties of silicon nanowires *Semicond. Sci. Technol.* **25** 024003
[9] Wagner R S and Ellis W C 1964 Vapor–liquid–solid mechanism of single crystal growth *Appl. Phys. Lett.* **4** 2
[10] Kayes B M, Filler M A, Putnam M C, Kelzenberg M D, Lewis N S and Atwater H A 2007 Growth of vertically aligned Si wire arrays over large areas (>1° cm[sup 2]) with Au and Cu catalysts *Appl. Phys. Lett.* **91** 103110
[11] Kolasinski K 2006 Catalytic growth of nanowires: vapor–liquid–solid, vapor–solid–solid, solution–liquid–solid and solid–liquid–solid growth *Curr. Opin. Solid State Mater. Sci.* **10** 182–91
[12] Putnam M C, Boettcher S W, Kelzenberg M D, Turner-Evans D B, Spurgeon J M, Warren E L, Briggs R M, Lewis N S and Atwater H A 2010 Si microwire-array solar cells *Energy Environ. Sci.* **3** 1037
[13] Kelzenberg M D, Turner-Evans D B, Putnam M C, Boettcher S W, Briggs R M, Baek J Y, Lewis N S and Atwater H A 2011 High-performance Si microwire photovoltaics *Energy Environ. Sci.* **4** 866
[14] Tsakalakos L, Balch J, Fronheiser J, Korevaar B A, Sulima O and Rand J 2007 Silicon nanowire solar cells *Appl. Phys. Lett.* **91** 233117
[15] Garnett E and Yang P 2008 Silicon nanowire radial p–n junction solar cells *J. Am. Chem. Soc.* **130** 9224–5
[16] Hannon J B, Kodambaka S, Ross F M and Tromp R M 2006 The influence of the surface migration of gold on the growth of silicon nanowires *Nature* **440** 69–71
[17] Zhang J, Li Y, Zhang X and Yang B 2010 Colloidal self-assembly meets nanofabrication: from two-dimensional colloidal crystals to nanostructure arrays *Adv. Mater.* **22** 4249–69
[18] Li X 2012 Metal assisted chemical etching for high aspect ratio nanostructures: a review of characteristics and applications in photovoltaics *Curr. Opin. Solid State Mater. Sci.* **16** 71–81
[19] Peng K-Q, Yan Y-J, Gao S-P and Zhu J 2002 Synthesis of large-area silicon nanowire arrays via self-assembling nanoelectrochemistry *Adv. Mater.* **14** 1164–7
[20] Schmitt S W, Schechtel F, Amkreutz D, Bashouti M, Srivastava S K, Hoffmann B, Dieker C, Spiecker E, Rech B and Christiansen S H 2012 Nanowire arrays in multicrystalline silicon thin films on glass: a promising

material for research and applications in nanotechnology *Nano Lett.* **12** 4050–4
[21] Wu B, Kumar A and Pamarthy S 2010 High aspect ratio silicon etch: a review *J. Appl. Phys.* **108** 051101
[22] Sökmen Ü, Stranz A, Fündling S, Merzsch S, Neumann R, Wehmann H H, Peiner E and Waag A 2010 Shallow and deep dry etching of silicon using ICP cryogenic reactive ion etching process *Microsyst. Technol.* **16** 863–70
[23] Henry M D, Walavalkar S, Homyk A and Scherer A 2009 Alumina etch masks for fabrication of high-aspect-ratio silicon micropillars and nanopillars *Nanotechnology* **20** 255305
[24] Ellinas K, Smyrnakis A, Malainou A, Tserepi A and Gogolides E 2011 'Mesh-assisted' colloidal lithography and plasma etching: a route to large-area, uniform, ordered nanopillar and nanopost fabrication on versatile substrates *Microelectron. Eng.* **88** 2547–51
[25] Zeniou A, Ellinas K, Olziersky A and Gogolides E 2014 Ultra-high aspect ratio Si nanowires fabricated with plasma etching: plasma processing, mechanical stability analysis against adhesion and capillary forces and oleophobicity *Nanotechnology* **25** 035302
[26] Welch C C, Goodyear A L, Wahlbrink T, Lemme M C and Mollenhauer T 2006 Silicon etch process options for micro- and nanotechnology using inductively coupled plasmas *Microelectron. Eng.* **83** 1170–3
[27] Tachi S 1988 Low temperature reactive ion etching and microwave plasma etching of silicon *Appl. Phys. Lett.* **52** 3
[28] de Boer M, Gardeniers J, Jansen H, Smulders E, Gilde M-J, Roelofs G and Elwenspoek M 2002 Guidelines for etching silicon MEMS structures using fluorine high-density plasmas at cryogenic temperatures *J. Microelectromech. Syst.* **11** 17
[29] Dussart R, Boufnichel M, Marcos G, Lefaucheux P, Basillais A, Benoit R, Tillocher T, Mellhaoui X, Estrade-Szwarckopf H and Ranson P 2004 Passivation mechanisms in cryogenic SF_6/O_2 etching process *J. Micromech. Microeng.* **14** 190–6
[30] Sökmen Ü, Stranz A, Fündling S, Wehmann H H, Bandalo V, Bora A, Tornow M, Waag A and Peiner E 2009 Capabilities of ICP-RIE cryogenic dry etching of silicon: review of exemplary microstructures *J. Micromech. Microeng.* **19** 105005
[31] Dussart R, Tillocher T, Lefaucheux P and Boufnichel M 2014 Plasma cryogenic etching of silicon: from the early days to today's advanced technologies *J. Phys. D: Appl. Phys.* **47** 123001
[32] Peng K, Xu Y, Wu Y, Yan Y, Lee S T and Zhu J 2005 Aligned single-crystalline Si nanowire arrays for photovoltaic applications *Small* **1** 1062–7
[33] Tsakalakos L *et al* 2007 Strong broadband optical absorption in silicon nanowire films *NANOP* **1** 013552
[34] Muskens O, Rivas J, Algra R, Bakkers E and Lagendijk A 2008 Design of light scattering in nanowire materials for photovoltaic applications *Nano Lett.* **8** 2638–42
[35] Hu L and Chen G 2007 Analysis of optical absorption in silicon nanowire arrays for photovoltaic applications *Nano Lett.* **7** 4
[36] Lin C and Povinelli M 2009 Optical absorption enhancement in silicon nanowire arrays with a large lattice constant for photovoltaic applications *Opt. Express* **17** 11
[37] Huang Y F *et al* 2007 Improved broadband and quasi-omnidirectional anti-reflection properties with biomimetic silicon nanostructures *Nat. Nanotechnology* **2** 770–4
[38] Chattopadhyay S, Chen L-C and Chen K-H 2006 Nanotips: growth, model, and applications *Crit. Rev. Solid State Mater. Sci.* **31** 15–53
[39] Lin C and Povinelli M 2011 Optimal design of aperiodic, vertical silicon nanowire structures for photovoltaics *Opt. Express* **19** 7
[40] Li J, Yu H, Wong S M, Li X, Zhang G, Lo P G-Q and Kwong D-L 2009 Design guidelines of periodic Si nanowire arrays for solar cell application *Appl. Phys. Lett.* **95** 243113
[41] Bao H and Ruan X 2010 Optical absorption enhancement in disordered vertical silicon nanowire for photovoltaic applications *Opt. Lett.* **35** 3378–80
[42] Du Q G, Kam C H, Demir H V, Yu H Y and Sun X W 2011 Broadband absorption enhancement in randomly positioned silicon nanowires for solar cell applications *Opt. Lett.* **36** 1884–6
[43] Street R A, Wong W S and Paulson C 2009 Analytic model for diffuse reflectivity of silicon nanowire mats *Nano Lett.* **9** 3494–7
[44] Makarona E, Skoulikidou M C, Kyrasta T, Smyrnakis A, Zeniou A, Gogolides E and Tsamis C 2015 Controllable fabrication of bioinspired three-dimensional ZnO/Si nanoarchitectures *Mater. Lett.* **142** 211–6
[45] Vijaya-Kumar M K, Constantoudis V, Gogolides E, Pret A V and Gronheid R 2012 Contact edge roughness metrology in nanostructures: frequency analysis and variations *Microelectron. Eng.* **90** 126–30
[46] Gantzounis G and Stefanou N 2006 Layer-multiple-scattering method for photonic crystals of nonspherical particles *Phys. Rev.* B **73** 035115
[47] Stefanou N, Yannopapas V and Modinos A 2000 MULTEM 2: a new version of the program for transmission and band-structure calculations of photonic crystals *Comput. Phys. Commun.* **132** 189–96
[48] Stefanou N, Yannopapas V and Modinos A 1998 Heterostructures of photonic crystals: frequency bands and transmission coefficients *Comput. Phys. Commun.* **113** 49–77
[49] Almpanis E and Papanikolaou N 2013 Designing photonic structures of nanosphere arrays on reflectors for total absorption *J. Appl. Phys.* **114** 083106
[50] Beeby J L 1968 The diffraction of low-energy electrons by crystals *J. Phys. C: Solid State Phys.* **1** 82
[51] Gonis A 1992 *Green Functions for Ordered and Disordered Systems* (Amsterdam: North-Holland)
[52] Yannopapas V, Modinos A and Stefanou N 1999 Optical properties of metallodielectric photonic crystals *Phys. Rev.* B **60** 5359–65
[53] Yannopapas V 2007 Negative refraction in random photonic alloys of polaritonic and plasmonic microspheres *Phys. Rev.* B **75** 035112
[54] Craciun G, Blauw M A, van der D E, Sarro P M and French P J 2002 Temperature influence on etching deep holes with SF_6/O_2 cryogenic plasma *J. Micromech. Microeng.* **12** 5
[55] Zijlstra T, van der D E, de Dood M J A, Snoeks E and Polman A 1999 Fabrication of two-dimensional photonic crystal waveguides for 1.5 μm in silicon by deep anisotropic dry etching *J. Vac. Sci. Technol.* B **17** 2734
[56] Yao L and He J 2014 Recent progress in antireflection and self-cleaning technology—from surface engineering to functional surfaces *Prog. Mater. Sci.* **61** 94–143
[57] Wang H P, Lai K Y, Lin Y R, Lin C A and He J H 2010 Periodic si nanopillar arrays fabricated by colloidal lithography and catalytic etching for broadband and omnidirectional elimination of Fresnel reflection *Langmuir: ACS J. Surf. Colloids* **26** 12855–8
[58] Aspnes D E 1988 *Properties of Silicon* (London: Inspec IEE)
[59] Seo K, Wober M, Steinvurzel P, Schonbrun E, Dan Y, Ellenbogen T and Crozier K B 2011 Multicolored vertical silicon nanowires *Nano Lett.* **11** 1851–6

[60] Chutinan A and John S 2008 Light trapping and absorption optimization in certain thin-film photonic crystal architectures *Phys. Rev.* A **78** 023825
[61] Peretti R, Gomard G, Seassal C, Letartre X and Drouard E 2012 Modal approach for tailoring the absorption in a photonic crystal membrane *J. Appl. Phys.* **111** 123114
[62] Spinelli P, Verschuuren M A and Polman A 2012 Broadband omnidirectional antireflection coating based on subwavelength surface Mie resonators *Nat. Commun.* **3** 692
[63] Sturmberg B, Dossou K, Botten L, Asatryan A, Poulton C, de Sterke M and McPhedran R 2011 Modal analysis of enhanced absorption in silicon nanowire arrays *Opt. Express* A **19** 15
[64] Fan S and Joannopoulos J D 2002 Analysis of guided resonances in photonic crystal slabs *Phys. Rev.* B **65** 235112
[65] Jin H, Citrin D S, Huaming W, Dingshan G, Zhiping Z and Shaoping C 2012 Slab-thickness dependence of photonic bandgap in photonic-crystal slabs *IEEE J. Sel. Top. Quantum Electron.* **18** 1636–42
[66] Khorasaninejad M, Abedzadeh N, Walia J, Patchett S and Saini S S 2012 Color matrix refractive index sensors using coupled vertical silicon nanowire arrays *Nano Lett.* **12** 4228–34
[67] Khorasaninejad M, Patchett S, Sun J, Nixon O and Saini S S 2013 Diameter dependence of polarization resolved reflectance from vertical silicon nanowire arrays: evidence of tunable absorption *J. Appl. Phys.* **114** 024304
[68] Patchett S, Khorasaninejad M, Nixon O and Saini S S 2013 Effective index approximation for ordered silicon nanowire arrays *J. Opt. Soc. Am.* B **30** 306–13
[69] Xie W Q, Oh J I and Shen W Z 2011 Realization of effective light trapping and omnidirectional antireflection in smooth surface silicon nanowire arrays *Nanotechnology* **22** 065704
[70] Sainiemi L, Jokinen V, Shah A, Shpak M, Aura S, Suvanto P and Franssila S 2011 Non-reflecting silicon and polymer surfaces by plasma etching and replication *Adv. Mater.* **23** 122–6
[71] Diedenhofen S L, Janssen O T A, Grzela G, Bakkers E P A M and Gómez R J 2011 Strong geometrical dependence of the absorption of light in arrays of semiconductor nanowires *ACS Nano* **5** 2316–23
[72] Jung J-Y, Guo Z, Jee S-W, Um H-D, Park K-T and Lee J-H 2010 A strong antireflective solar cell prepared by tapering silicon nanowires *Opt. Express* A **18** 286–92
[73] Fan Z *et al* 2010 Ordered arrays of dual-diameter nanopillars for maximized optical absorption *Nano Lett.* **10** 3823–7